Fabrication of InP-based monolithically integrated laser transmitters

Article *in* Science China Information Sciences · August 2018

DOI: 10.1007/s11432-018-9478-1

7 authors, including:

Song Liang
Chinese Academy of Sciences
120 PUBLICATIONS **795** CITATIONS
SEE PROFILE

Dan Lu
institute of semiconductors
189 PUBLICATIONS **941** CITATIONS
SEE PROFILE

Lingjuan Zhao
Chinese Academy of Sciences
240 PUBLICATIONS **1,235** CITATIONS
SEE PROFILE

Hongliang Zhu
Andrews University
136 PUBLICATIONS **880** CITATIONS
SEE PROFILE

SCIENCE CHINA
Information Sciences

• REVIEW •

August 2018, Vol. 61 080405:1–080405:19
https://doi.org/10.1007/s11432-018-9478-1

Special Focus on Photonic Devices and Integration

Fabrication of InP-based monolithically integrated laser transmitters

Song LIANG[1,2,3*], Dan LU[1,2,3], Lingjuan ZHAO[1,2,3*], Hongliang ZHU[1,2,3], Baojun WANG[1,2,3], Daibing ZHOU[1,2,3] & Wei WANG[1,2,3]

[1]*Key Laboratory of Semiconductor Materials Science, Institute of Semiconductors, Chinese Academy of Sciences, Beijing* 100083*, China;*
[2]*College of Materials Science and Opto-Electronic Technology, University of Chinese Academy of Sciences, Beijing* 100083*, China;*
[3]*Beijing Key Laboratory of Low Dimensional Semiconductor Materials and Devices, Institute of Semiconductors, Chinese Academy of Sciences, Beijing* 100083*, China*

Received 18 February 2018/Revised 2 May 2018/Accepted 16 May 2018/Published online 9 July 2018

Abstract InP-based photonic integrated circuits (PICs) have aroused great interest in recent years to meet the needs of future high-capacity and high-performance optical systems. With the advantages of small size, low power consumption, low cost, high reliability, InP-based PICs are promising solutions to replace the multiple discrete devices used in various systems. In this paper, we will review the design, fabrication, key integration technology and performance of several kinds of InP-based monolithically integrated transmitters developed in our group in recent years. Particular attention will be paid to the electro-absorption modulated laser (EML), multi-wavelength distributed feedback (DFB) laser arrays, widely tunable distributed reflector (DBR) lasers and their arrays, integrated amplified feedback lasers (AFL), and few-mode transmitters.

Keywords photonic integration, EMLs, multi-wavelength DFB laser arrays, widely tunable DBR lasers, integrated AFL, few-mode transmitters

Citation Liang S, Lu D, Zhao L J, et al. Fabrication of InP-based monolithically integrated laser transmitters. Sci China Inf Sci, 2018, 61(8): 080405, https://doi.org/10.1007/s11432-018-9478-1

1 Introduction

The capacity of optical fiber communication networks has been increasing rapidly with the explosive growth of the Internet [1]. To meet the requirements of future high-performance optical networks, InP-based photonic integrated circuits (PICs) have been developed in recent years. Many types of InP-based PICs have been demonstrated, typical of which includes tunable optical routers [2], multi-channel transmitters [3] /monitors [4], and optical pulse shaper [5]. Comparing with multiple discrete devices used in optical systems, PICs have the advantages in small weight and size, low power consumption, low cost, better functionality and high scalability. Besides InP-based monolithic PICs, silicon-based PICs have also been investigated extensively [6–8], in which gain chips are usually based on InP materials. Although great achievements have been made in silicon devices, the transceiver market is still dominated by InP-based devices, which will also lead the market in next ten years[1)] [9]. InP-based PICs will also be of great value in both research and industry fields. Leading universities, research institutes, and companies

* Corresponding author (email: liangsong@semi.ac.cn, ljzhao@semi.ac.cn)
1) Integrated optical devices. https://www.lightcounting.com/Silicon.cfm.

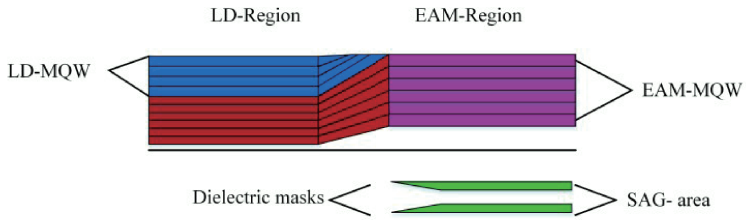

Figure 1 (Color online) Schematic material structure of an EML fabricated using our novel process.

worldwide are investing much into the development of InP-based PICs to achieve more functionality and higher integration density.

In this paper, we will review the design, fabrication, and performance of several kinds of InP-based monolithically integrated transmitters developed in our group at Institute of Semiconductors, Chinese Academy of Sciences. Particular attention will be paid to the electroabsorption modulated lasers (EML), multi-wavelength laser arrays, widely tunable distributed reflector (DBR) lasers and arrays, integrated amplified feedback lasers (AFL), and few-mode transmitters.

2 Integration techniques

In this section, two key integration techniques based on metal organic chemical vapor deposition (MOCVD), the selective area growth (SAG) technique and the butt-joint technique, will be briefly described.

In the SAG process [10,11], SiO_2 mask stripes are formed on the substrate first before material growth. During the following MOCVD process, no material is nucleated or grown on the SiO_2 masks, and the deposition of semiconductor material happens only in the areas with no SiO_2 masks. The growth rate of the material in the wafer areas between the masks is enhanced, and the composition of the material is also different from that on bare substrates. For bulk material, the SAG process leads to mainly an effective refractive index change resulted from the thickness variation. For multi-quantum wells (MQWs), because the emission wavelength is sensitive to the well thickness, a significant amount of wavelength tuning can be obtained besides the refractive index change. The butt-joint technique involves two MOCVD processes. In the first one, semiconductor materials such as MQWs are grown on the whole wafer. Then, with the protection of SiO_2 masks over some areas, the materials in other areas of the wafer are selectively removed by combing dry and wet etching. In the second MOCVD step, semiconductor materials having different parameters are butt-jointed with the materials grown in the first MOCVD step, which are protected with the SiO_2 masks. The advantage of the butt-joint technique is that the properties of the two butt-jointed materials can be optimized separately [12, 13]. Besides, the number of different kinds of materials that can be integrated on a single wafer has no limitation in principle.

3 Electroabsorption modulated laser

EML integrates an electroabsorption modulator (EAM) with a distributed feedback (DFB) laser on a single chip. Compared with configurations including discrete DFB lasers and EAMs, EMLs improve losses, reduce expense, and improve reliability by eliminating the coupling optics. To obtain bandgap wavelength tuning between the EAM material and laser material, both the SAG technique and the butt-joint technique can be used for the fabrication of EMLs. However, careful optimizations are needed to get high-quality butt-joint interface between the laser and butt-jointed materials [12]. In the SAG process, the optimal MQW parameters for high-performance EAMs and lasers cannot be obtained at the same time [14].

To fabricate high-performance EMLs, we developed a novel process to avoid the drawbacks in the SAG and butt-joint techniques [15, 16]. As shown in Figure 1, pairs of dielectric masks are formed in

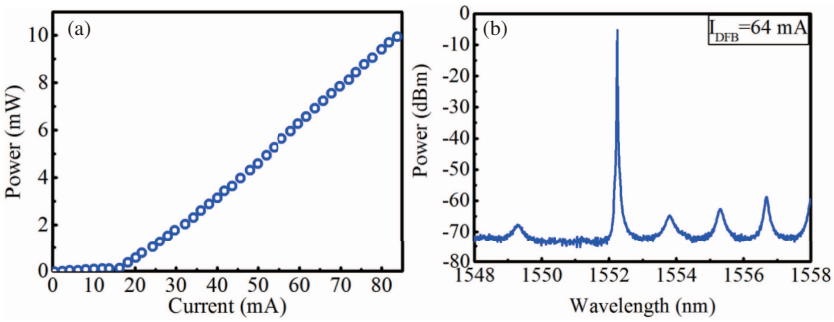

Figure 2 (Color online) Typical P-I characteristic (a) and optical spectrum (b) of an EML [16] @Copyright 2018 IEEE.

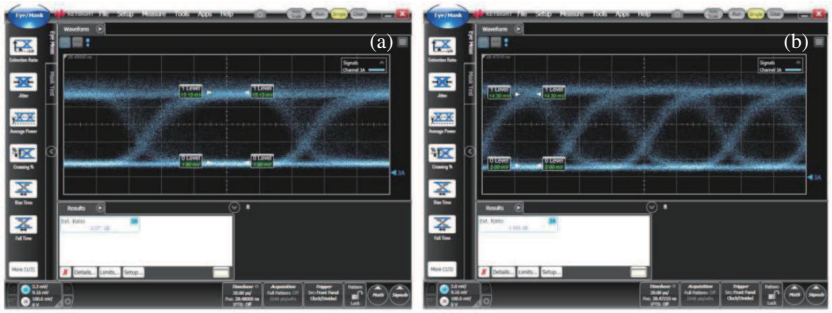

Figure 3 (Color online) Eye diagrams of an EML at 10 Gb/s (a) and 20 Gb/s (b) modulations in BTB configuration [16] @Copyright 2018 IEEE.

the EAM areas, instead of the laser areas as in the usual SAG method for EML fabrication. Then, on the patterned substrate, the EAM and laser MQWs are grown in a single MOCVD growth successively. After the growth, the laser MQWs in the EAM areas are removed selectively, leaving only the lower EAM MQWs in the areas. Similar to the usual SAG technique, both the modulator MQWs and laser MQWs can be obtained in only one epitaxy run. The difference is that the two MQW materials can be optimized separately because they are grown at different times. Additionally, because the SAG masks are placed in the EAM section, the bandgap wavelength of the bottom MQWs in the laser section can be set to be over 100 nm shorter than that of the upper laser MQWs. Thus the effects of the bottom MQWs on the laser performance can be reduced effectively.

Figure 2(a) shows a typical light power vs. injection current (P-I) characteristic of an EML fabricated by the above process. The threshold current at room temperature is about 16 mA. The output power is larger than 10 mW at laser section current of 85 mA. The typical optical spectrum is shown in Figure 2(b). The side mode suppression ratio (SMSR) is over 50 dB. The 10-Gb/s and 20-Gb/s eye diagrams of the chip are shown in Figure 3. Clear-opened eyes can be obtained under both conditions. The dynamic extinction ratios (DER) are 9.1 and 8.6 dB, for the 10-Gb/s and 20-Gb/s modulation, respectively.

4 DFB laser arrays

Monolithically integrated multi-wavelength DFB laser arrays (MWLAs) are important light sources for modern wavelength division multiplexing (WDM) optical communication systems. Compared with multiple discrete lasers, MWLAs have lower packaging cost, lower power consumption and compact size [17,18]. To fabricate MWLAs, different laser emissions which are typically uniformly spaced have to be defined side by side on a wafer. The uniformity of the wavelength spacing influences the yield of laser arrays greatly [17]. Up to now, there are several techniques available for the fabrication of MWLAs, including electron beam lithography (EBL) [17], ridge width variation [19], and multiple holographic exposures [20]. EBL is the most widely known one, by which different wavelengths are obtained by varying the pitch of DFB gratings in an array [17]. However, the EBL equipment is expensive and the EBL process is rather

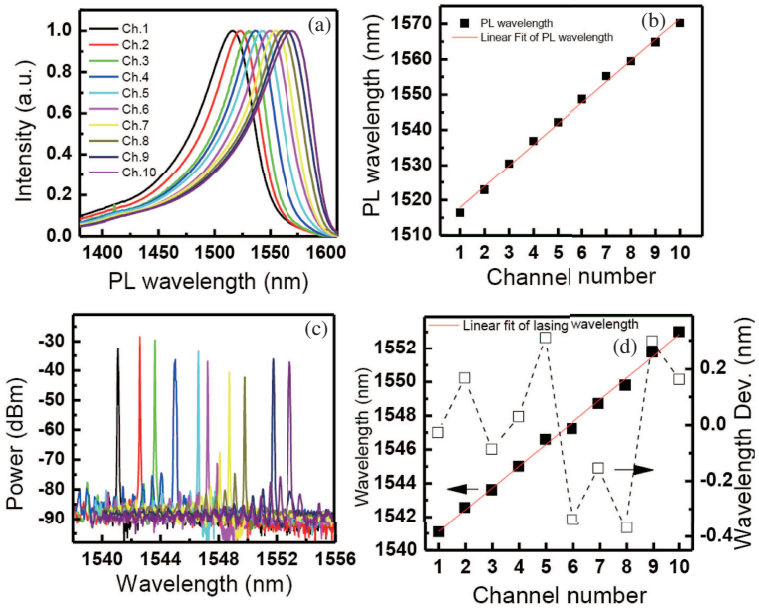

Figure 4 (Color online) (a) PL spectra and (b) peak wavelength of the SAG MQWs; (c) laser spectra and (d) emission wavelengths and wavelength residues with respect to corresponding linear fitting values of DFB lasers in an array fabricated by SAG of MQWs [21] @Copyright 2013 Elsevier.

time-consuming, which lead to a low throughput and a high cost of laser arrays. Besides, the limited resolution of typical EBL makes it a challenge for the fabrication of WDM laser arrays which have less than 1-nm channel spacings. We fabricate MWLAs by using SAG technique [10, 11], which needs only a simple procedure and thus has the benefits of low cost and is suitable for mass production. In the SAG process, dielectric mask strips are used to tune the effective index (neff) of the laser material. By adopting DFB gratings with a uniform pitch (Λ), different emission wavelengths in a laser array can be achieved according to $\lambda = 2n_{\rm eff}\Lambda$.

4.1 Fabrication of MWLAs by SAG of MQWs

When MWLAs are fabricated by SAG of MQWs, a SiO_2 layer is first deposited on an InP wafer by plasma enhanced chemical vapor deposition (PECVD) [21–24]. Parallel pairs of mask strips with a period, which is equal to the separation between two adjacent lasers in a laser array, are patterned by photolithography and HF wet etching. MQWs and both the upper and lower separate confinement heterostructure (SCH) layers are then grown on the patterned wafer in the following MOCVD step. Figure 4(a) shows the photoluminescence (PL) spectra of the MQWs of a ten-channel laser array obtained by the SAG process. The width of the gap between each mask pair is kept at 20 μm, and the width of the mask strips is ranged from 4.35 to 20.01 μm with a step of 1.74 μm. As is shown in Figure 4(a), the peak PL wavelength increases with the mask width (channel number) gradually. This change in wavelength is attributed to the increase of the MQW thickness, which is accompanied by a corresponding effective refractive index change from laser to laser in an array. After the DFB grating with a uniform pitch is fabricated by holographic lithography technology, ten different emission wavelengths can be obtained as shown in Figure 4(c). The laser array has a 1.29-nm average channel spacing. The wavelength deviations from the corresponding linear fitted values are less than 0.4 nm.

Besides forming multi-wavelength emission, the SAG of MQWs can also be used for the integration of other optical components such as EAMs with laser arrays at the same time [25, 26]. Figure 5 shows a fabricated ten-channel electroabsorption modulated DFB laser array. In the EAM region of the device, where there are no SAG masks, the PL peak wavelength of the MQWs is about 1500 nm. Because of the presence of the SAG mask, the PL peak wavelengths of the MQWs of the lasers are longer and are ranged from 1530 to 1580 nm as the mask width increases. As shown in Figure 5, an arrayed waveguide

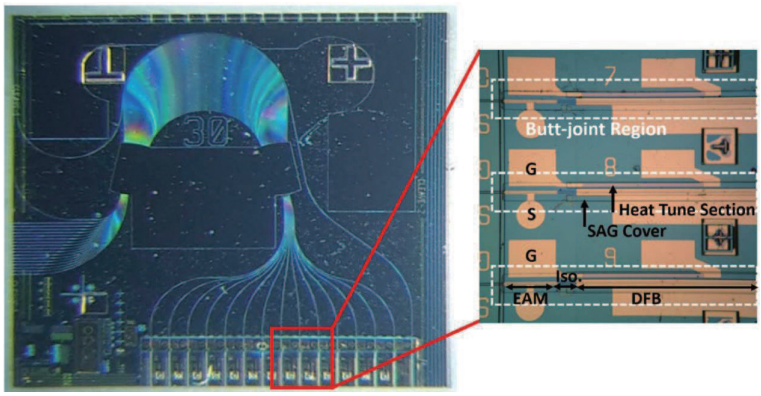

Figure 5 (Color online) A ten-channel EML laser array fabricated by SAG of MQWs [26] @Copyright 2017 Elsevier.

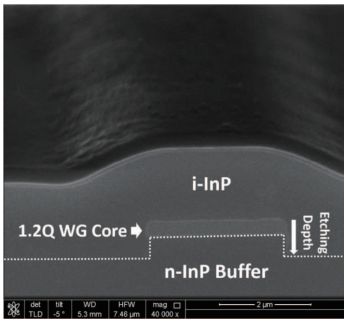

Figure 6 SEM picture of a buried passive waveguide [26] @Copyright 2017 Elsevier.

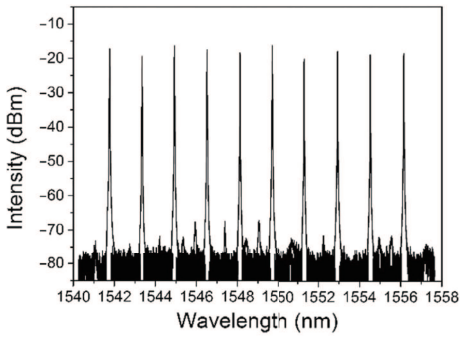

Figure 7 Laser spectra of an EML array fabricated by SAG of MQWs [26] @Copyright 2017 Elsevier.

grating (AWG) combiner having InGaAsP waveguide core with 1.2-μm PL peak wavelength is integrated monolithically with the laser array by butt-joint regrowth technique. A buried ridge waveguide structure is adopted for the passive waveguides as shown in Figure 6. A self-aligned fabrication procedure is adopted for the fabrication of the waveguide structure to eliminate the misalignment between the laser active waveguide and the passive waveguide [26]. A Ti thin film heater is integrated for each laser in the array. As shown in Figure 7, a uniform wavelength channel spacing (1.8 nm) can be obtained with the help of the integrated heaters. The integrated EAMs have a static extinction ratio larger than 11 dB and small signal modulation bandwidth over 8 GHz. The light power collected at the output waveguide of the AWG is larger than −13 dBm for each wavelength.

4.2 Fabrication of MWLAs by SAG of upper SCH layer

As shown above, in the MQW SAG process, the material layers affected by the SAG include both the two SCH layers and the MQWs, which induces several problems. First, the PL peak wavelengths of the SAG MQWs change more rapid than the emission wavelengths of the DFB lasers which are determined by neff of the laser material. Then, because of the SAG process, the thickness, composition, and state of strain of the SAG materials vary from laser to laser in an array [21]. This will inevitably lead to the deviation of the material parameters from the optimized values, causing deterioration of the material quality of some lasers. These aspects may result in nonuniform performance among different lasers in a laser array. What is more, the ability to control the wavelength spacing may also be impaired. The uniformity of wavelength spacing of the laser arrays fabricated by MQW SAG technique as shown in Figure 4 needs to be further improved.

To fabricate high-quality MWLAs, we propose a modified SAG technique [27, 28]. Different from the conventional MQW SAG procedure, in which dielectric masks are formed on the buffered substrates, to fabricate MWLAs with our modified SAG technique, a buffer layer, a lower SCH layer and an MQW layer

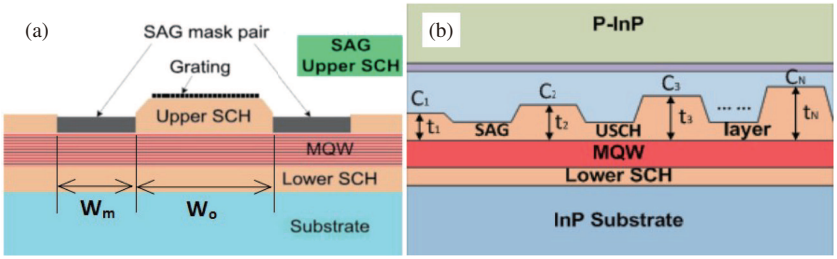

Figure 8 (Color online) (a) Schematic process of SAG of upper SCH layer; (b) schematic structure of fabricated laser array.

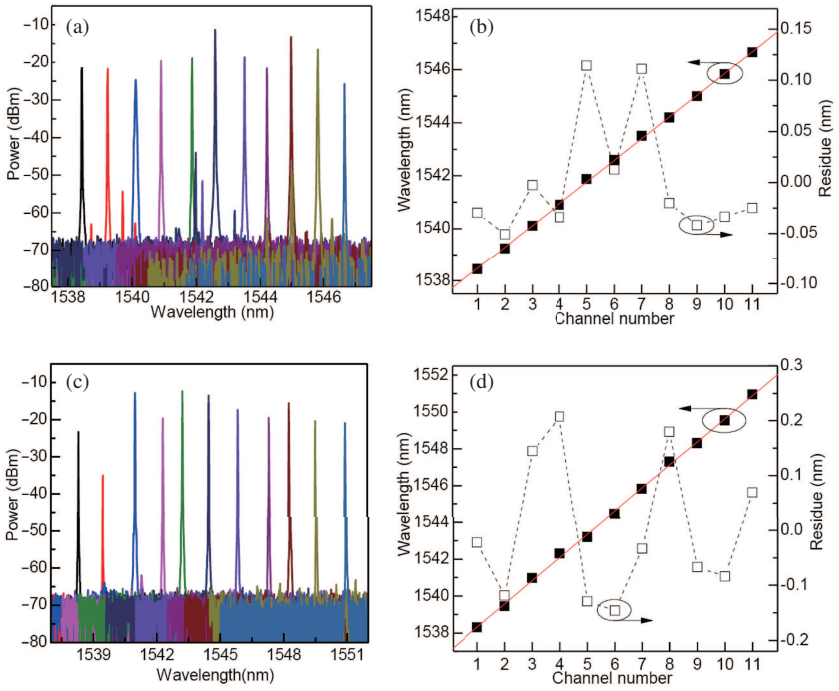

Figure 9 (Color online) Measured spectra and laser wavelengths of the laser arrays fabricated by SAG of SCH layer, (a) and (b) are for the 0.8 nm arrays; (c) and (d) are for the 1.25 nm laser arrays [27] @Copyright 2012 OSA.

are first grown on the substrates. Then mask strip pairs with gradually changed dimensions are formed on the MQW layer. In the following SAG step, just an upper SCH layer is grown, and the thickness of only the layer is changed by the SAG masks to obtain different Bragg wavelengths, as shown schematically in Figure 8. The materials including the lower SCH layer and especially the MQW layer whose properties are sensitive to different growth conditions are left untouched, resulting in precise control of the wavelength spacing.

DFB Laser arrays having 0.8 and 1.25 nm average channel spacings are fabricated through increasing the width of the SAG strips ((W_m) in Figure 8(a)) from 0 μm by 3-μm and 1.5-μm steps, respectively. The separation between two mask strips is 20 μm (W_o in Figure 8(a)). As a result, the thickness differences of the upper SCH layer (Figure 8(b)) between each two adjacent lasers are 4 and 2 nm, respectively, for the 0.8 and 1.25 nm spacing arrays. The spectra are shown in Figure 9(a) and (c), respectively. The measured laser wavelength increases with the channel number with very good linearity for both the arrays, as can be seen from Figure 9(b) and (d). The wavelength residues with respect to the corresponding linear fitting values are between −0.05 and +0.11 nm, and −0.14 and +0.2 nm, respectively, for the 0.8 and 1.25 nm laser arrays. The standard deviation of the residue distribution is 0.0672 nm, which is smaller than those (0.1 nm) of MWLAs fabricated by other techniques including EBL. Because the MQWs are not affected, the laser elements in the arrays have uniform P-I characteristics with threshold currents

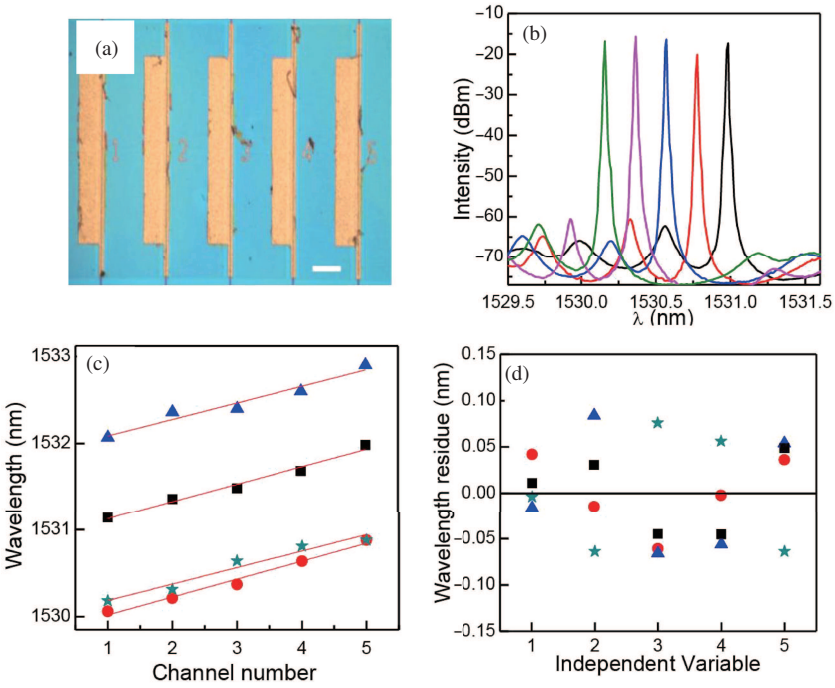

Figure 10 (Color online) (a) Optical graph of a laser array, (b) typical optical spectrum, (c) emission wavelength and (d) wavelength residue with respect to linear fitting values [29] @Copyright 2016 IEEE.

around 18 mA.

Besides accurate wavelength spacings, another important issue for the fabrication of MWLAs is a high single-mode yield of the DFB laser elements. MWLAs with a 25-GHz channel spacing has been fabricated by combining the SCH SAG technique and the REC technique [29], in which an equivalent phase shift can be introduced to ensure single mode lasing of DFB lasers [30]. Only conventional photolithography is needed to conduct both the SAG and REC processes. Thus a low fabrication cost of our laser arrays can be expected. The measured emission properties of fabricated 5-channel laser arrays are shown in Figure 10. As can be seen, the increase of the laser wavelength with the channel number for all the arrays shows good linearity. As is shown in Figure 10(c), the wavelength residues with respect to linear fitting values for all the lasers are within −0.1 and +0.1 nm with a 0.051 nm standard deviation. It is worth noting that MWLAs with this small channel spacing cannot be fabricated by standard commercial EBL facility through varying the pith of DFB gratings because of the resolution limitation. It is a unique advantage of our SCH SAG technique if the channel spacings of MWLAs are required to be smaller than 0.8 nm.

For MWLAs, an integrated optical combiner will facilitate the fiber coupling greatly. By combining the SCH SAG technique and the bundle integrated guide (BIG) technique [31], both multi-wavelength emission with highly uniform spacing and low loss passive waveguide material can be obtained in a single MOCVD step [32], which simplifies the fabrication of combiner integrated arrays greatly. A top view microscope image of a fabricated device is shown in Figure 11(a). The device consists of a DFB laser array section, a multimode interference (MMI) combiner section, and a semiconductor optical amplifier (SOA) section. A three-step MOCVD process is needed for the fabrication of the device. In the first MOCVD step, an InGaAsP lower SCH layer lattice matched to InP, a 20-nm InP etch stop layer, and an MQW layer are grown on the substrates. Then, SiO_2 mask strip pairs with gradually changed dimensions for different laser elements are formed on the MQW layer in only the laser areas of the wafer. The MQW layer and the etch stop layer in the passive waveguide regions are then selectively removed by wet etching as shown schematically in Figure 11(b).

In the second MOCVD step, an undoped InGaAsP upper SCH layer lattice-matched to InP is grown on the patterned wafer. The schematic structure of the obtained wafer is shown in Figure 11(c). In the

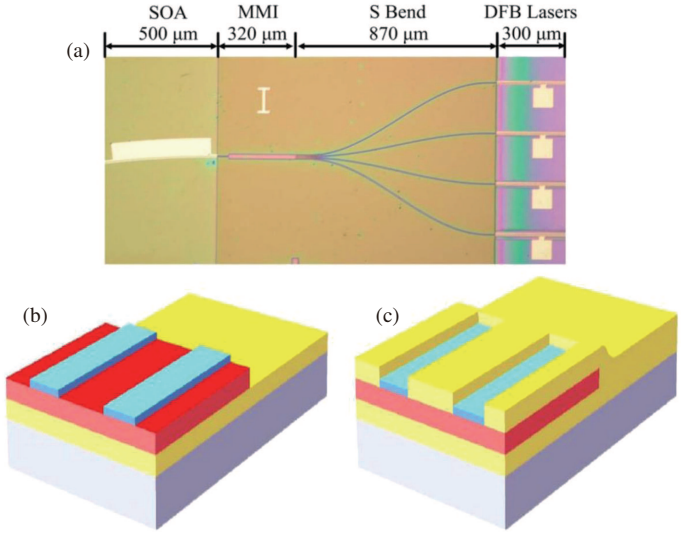

Figure 11 (Color online) (a) Microscope graph of a laser array. Two of the fabrication processes are shown in (b) and (c), respectively [32] @Copyright 2015 IEEE.

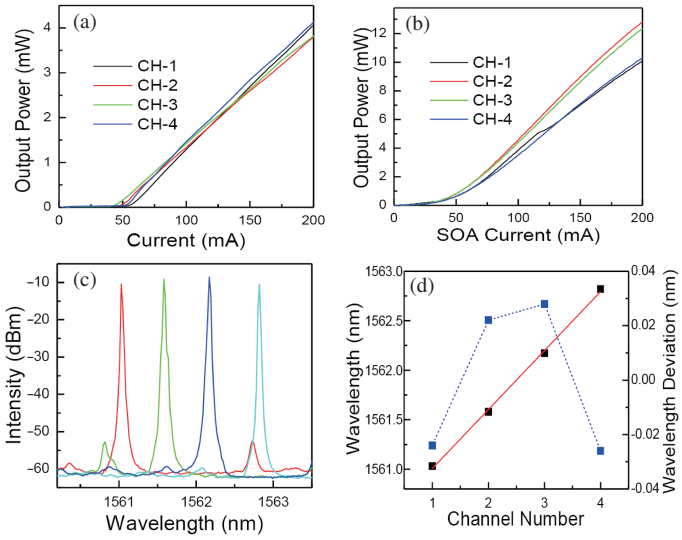

Figure 12 (Color online) 12 Light output (a) and (b), spectra (c) and wavelength (d) properties of the laser array [32] @Copyright 2015 IEEE.

laser areas of the wafer, the upper SCH layer grown in the second MOCVD step is modulated by the SiO_2 patterns to get different emission wavelengths. Except for the SiO_2 patterns, the above process is the same as that of the BIG process [31]. In the passive waveguide regions, both the lower SCH layer grown in the first MOCVD step and the upper SCH layer grown in the second MOCVD step form the core layer of the passive waveguides, which has a total thickness of more than 200 nm. The emission wavelength of 1.2 μm from the InGaAsP SCH layers is far away from the laser wavelength, resulting in a very low absorption loss. The lasing properties of the device are shown in Figure 12. With the help of the integrated SOA, each laser channel has a light power larger than 10 mW when working individually. The laser array has a channel spacing of 0.6 nm with a very good uniformity as expected.

5 Tunable DBR lasers and laser arrays

The introduction of WDM into passive optical networks (WDM-PONs) is a promising way to increase the capacity of optical access networks [33, 34]. For the large number of optical network units (ONUs)

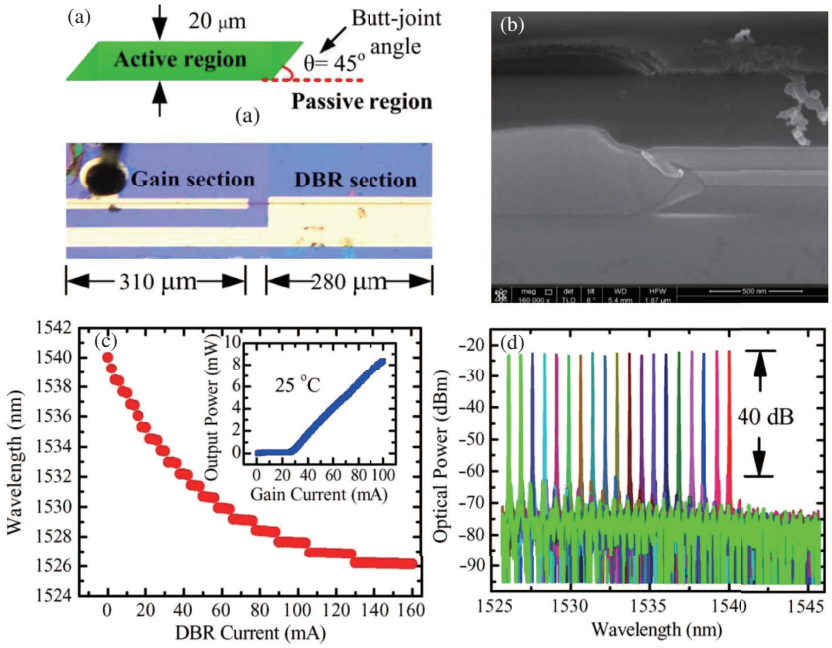

Figure 13 (Color online) (a) Optical graph of a DBR laser and shape of a mask for the butt-joint growth; (b) SEM picture of a butt-joint interface; (c) tuning properties; (d) typical spectra [41] @Copyright 2014 IEEE.

in WDM-PONs, colorless transmitters are highly desired so that the costs related to the inventory and management of the transmitters can be reduced greatly. One of the available colorless light sources for WDM-PONs is wavelength tunable laser, the application of which is considered as the easiest way to realize colorless ONUs [35]. WDM-PONs with tunable lasers have superior properties such as remarkable simplicity and reliability, and remote management of the wavelength plan of the network [35].

Compared with other InP-based tunable lasers such as sampled grating (SG) DBR lasers [36], InP-based two or three section DBR lasers [37,38] have a simpler structure. It can be easily calibrated because the number of controlling currents for a wavelength is reduced. The calibration time of the two or three section DBR lasers can thus be much shorter, making it more suitable for mass production. Besides, the less controlling parameters lead to a simpler wavelength locking algorithms. These features make the DBR lasers promising in future high capacity WDM-PONs.

5.1 Widely tunable directly modulated DBR lasers

For WDM optical communication applications, a wider wavelength tuning range is desired so that the capacity of the systems can be increased by incorporating more data channels. In DBR lasers, the effective refractive index of the material of the DBR grating section is decreased when a current is injected in the section, leading to a blueshift of the emission wavelength. For material with a narrower bandgap, the changing rate of the index is higher, and the total amount of the index change before saturation is larger [39]. We thus fabricate DBR lasers which have long wavelength InGaAsP as DBR material to get a wide wavelength tuning range [40,41]. Figure 13(a) shows the microscope image of a finished DBR laser, which has a gain section and a DBR section. InGaAsP MQWs are used as the gain material. A 400-nm thick InGaAsP material with 1.4-μm PL peak wavelength (1.4 Q) is butt-jointed as the DBR material. As shown in Figure 13(b), the laser emission wavelength can be tuned by 13.8 nm for a Bragg current of 160 mA at 40°C, which is notably larger than those of the DBR lasers fabricated by other techniques. Typical optical spectra obtained from the device are shown in Figure 13(c), with SMSR larger than 40 dB for all channels. The small signal modulation bandwidth of the DBR laser measured at 10°C are shown in Figure 14(a). The 3-dB bandwidths are larger than 10 GHz for different gain currents. 10-Gb/s data modulation experiments are also conducted. In the back to back condition, clear-opened eye diagrams can be obtained at different wavelength channels. As typical examples, eye diagrams measured at six

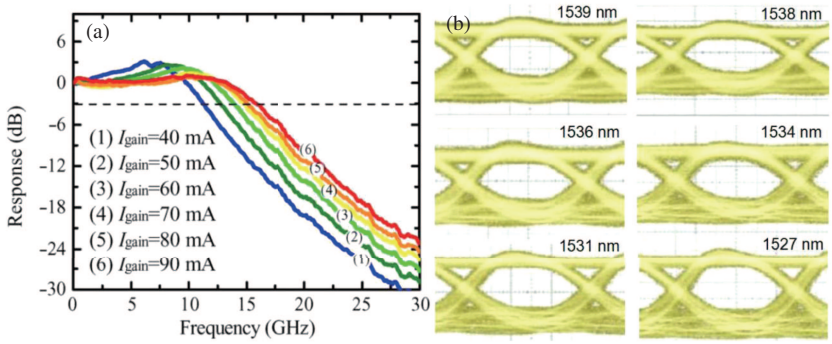

Figure 14 (Color online) (a) Small signal modulation response of the DBR laser; (b) typical 10-Gb/s eye diagrams [41] @Copyright 2014 IEEE.

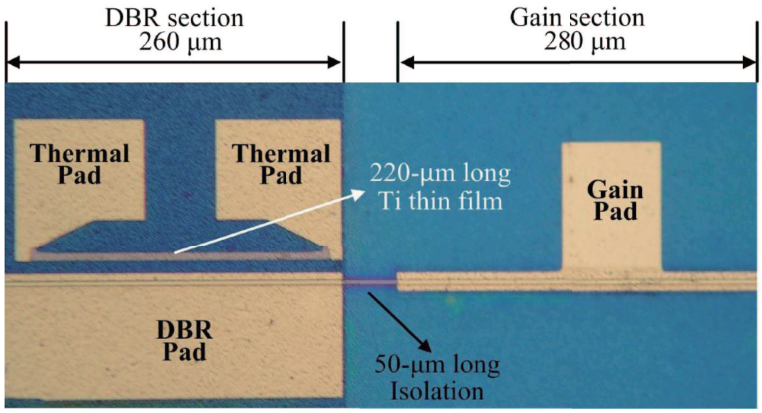

Figure 15 (Color online) A Ti heater integrated DBR laser [44] @Copyright 2016 IEEE.

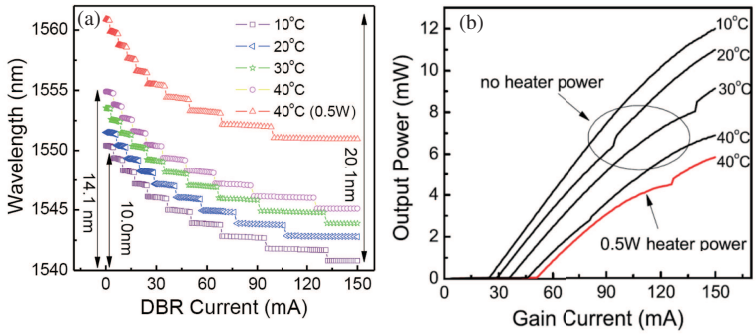

Figure 16 (Color online) (a) Wavelength tuning and (b) output power properties of the heater integrated DBR laser [44] @Copyright 2016 IEEE.

different wavelengths are shown in Figure 14(b).

To further increase the wavelength tuning range, a Ti thin film heater [42,43] can be integrated in the DBR section of the laser as shown in Figure 15 [44]. The width and length of the heater are 5 and 220 μm, respectively. The heater is positioned 10 μm away from the ridge waveguide of the device and has a 500-resistance. The wavelength tuning properties of the device is shown in Figure 16(a). Accompanied with the variation of the heatsink temperature, a 0.5-W heat power of the thin film heater helps to enlarge the wavelength tuning range to 20.1 nm, which is the largest one obtained from two or three section DBR lasers to the best of our knowledge. Because the heater locates only in the DBR section, which is over 50 μm away from the gain section, its heating effect on the gain section is small. As can be seen from Figure 16(b), to obtain the 6-nm tuning range enhancement with the 0.5 W heater power, the changes of the threshold current and the output power at 150-mA gain current is 6 and 1.1 mW, respectively, which

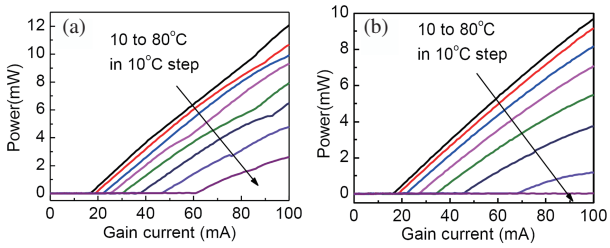

Figure 17 (Color online) Light output properties of InGaAlAs (a) and InGaAsP (b) DBR lasers [45] @Copyright 2017 OSA.

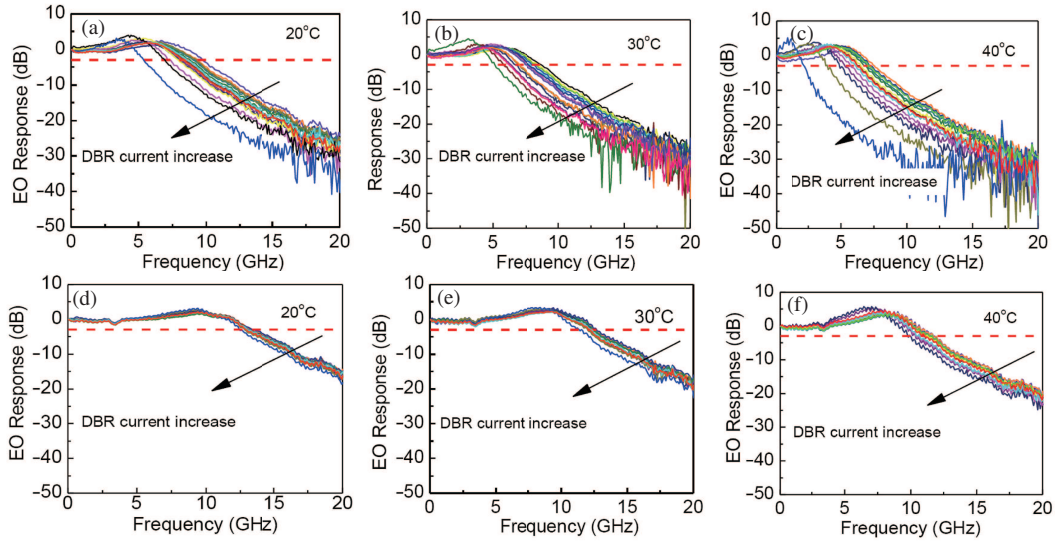

Figure 18 (Color online) Direct modulation response of InGaAlAs (a), (b), (c) and InGaAsP (d), (e), (f) DBR lasers [45] @Copyright 2017 OSA.

are noticeably smaller than the 33 and 5.1 mW during the 40°C temperature increase of the heat sink to get the 4-nm tuning enhancement.

The direct modulation properties of the DBR lasers with integrated heaters are also studied. It is found that the modulation bandwidth decreases rapidly with the increase of heat sink temperature and the heater power [44]. To get better performance at high temperature, we fabricate the first InP-based DBR laser [45] which has 1.4 Q as DBR material, but InGaAlAs MQWs as gain material, which are well known to yield improved high-temperature performance for lasers due to the more favourable conduction-band offset. The properties of the InGaAlAs DBR lasers are studied in comparison with the InGaAsP DBR lasers. As shown in Figure 17, the InGaAlAs DBR laser has higher output power and lower threshold current at high temperatures as expected. The direct modulation responses of the DBR lasers are shown in Figure 18. It can be seen that the modulation bandwidth decreases with the DBR current for both the two kinds of devices. An interesting observation is that the decrease in the bandwidth with the increase of the DBR current of the InGaAlAs laser is notably slower than that of the InGaAsP lasers. As can be seen from Figure 18(a) and (d), at 20°C, the bandwidth of the InGaAsP lasers decreases rapidly to 5.3 GHz as the DBR current increases to 60 mA. The decrease in the bandwidth for the InGaAsP DBR laser is 4.4 GHz, which is four times larger than the decrease in bandwidth for the InGaAlAs laser. The uniform modulation properties among different wavelength channels of the InGaAlAs DBR laser should be highly desirable for practical applications.

5.2 EAM modulated widely tunable DBR laser

Due to the small chirping characteristics, externally modulated lasers are more suitable for long-distance optical fiber communication systems than directly modulated lasers [46]. Figure 19(a) shows an EAM

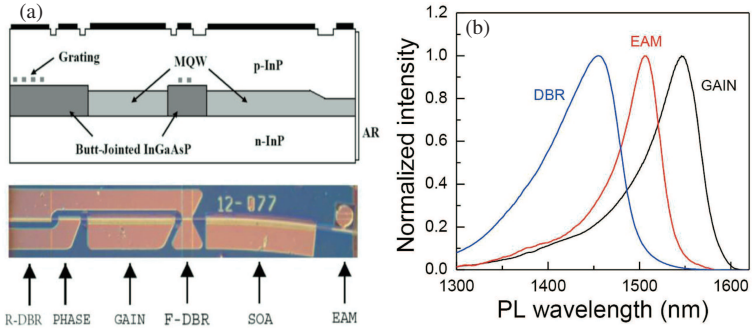

Figure 19 (Color online) (a) Schematic structure and microscope graph of an EAM modulated DBR laser; (b) PL spectra of materials in different device sections [46] @Copyright 2014 OSA.

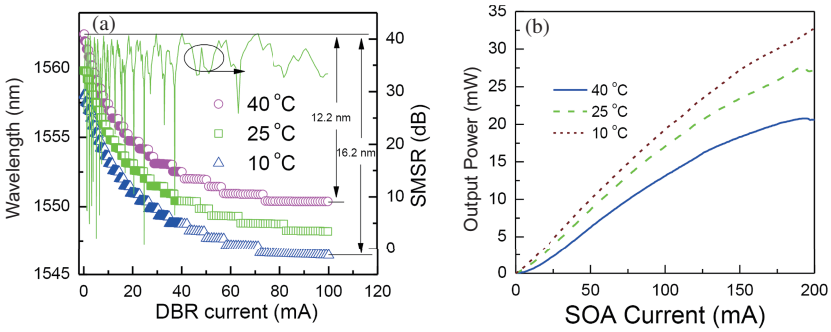

Figure 20 (Color online) (a) Tuning and (b) output power properties of the EAM modulated DBR laser [46] @Copyright 2014 OSA.

modulated widely tunable DBR laser, which consists of a four section DBR laser followed by a 500-μm SOA and a 150-μm EAM. The DBR laser includes a 200-μm rear mirror, a 100-μm phase section, a 400-μm gain section and a 50-μm front mirror. The waveguide is curved from the beginning of the SOA to reach a final facet angle of 7° to reduce the facet reflection. To get a large tuning range, 1.4-Q DBR material is used in the butt-jointed process. The EAM is integrated using the MQW SAG technique. The PL spectra of the gain, DBR and EAM section materials are shown in Figure 19(b).

Figure 20(a) shows the laser wavelength and the corresponding SMSR as functions of the DBR inject current and temperature. Accompanied by varying the chip temperature by 30 degrees (from 10°C to 40°C), a total tuning range of 16.2 nm is achieved, which is the largest for DBR transmitters of the same kind. As is shown, the SMSR is higher than 30 dB in the whole tuning range except in the regions where mode jump happens. The output power properties of the device are shown in Figure 20(b). At 10°C, the light power is larger than 30 mW with the help of the integrated SOA, which is the largest output power that has been obtained from similar DBR chips to the best of our knowledge, helping to improve the power budget and scalability of WDM-PONs.

The static extinction ratio curves of the integrated EAM of the device with up to 5-V reverse bias are shown in Figure 21(a). At 25°C, the device provides total extinction ratio of 28–32 dB for wavelengths from 1547 to 1557 nm. The small signal modulation response of the integrated EAM is shown in Figure 21(b). The measured 3-dB frequency bandwidths are around 13 GHz. The eye diagrams obtained from 10-Gb/s data modulation experiments are shown in Figure 22. Clear-opened eye diagrams can be obtained after 75-km of single mode fiber transmission. With the integrated EAM the reach distance of the PONs can be greatly extended.

5.3 EAM modulated DBR laser array

Recently FSAN (full service access network) community has selected TWDM (time and wavelength division multiplexed)-PONs as a key solution for future broadband PON systems[2)]. In such a system,

2) FSAN next generation PON task group. http://www.fsan.org/task-groups/ngpon/.

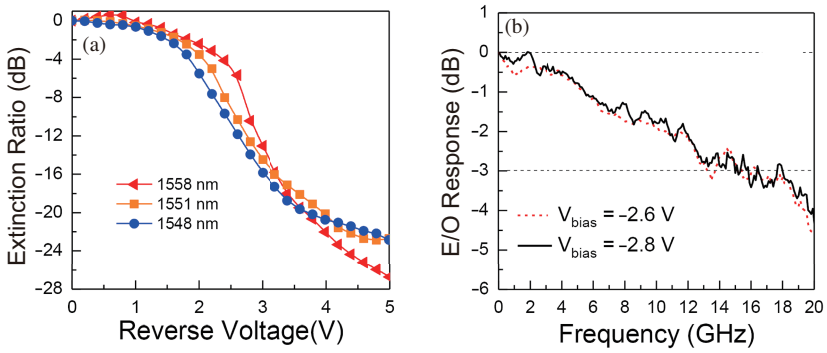

Figure 21 (Color online) (a) Static extinction and (b) small signal modulation properties of the EAM [46] @Copyright 2014 OSA.

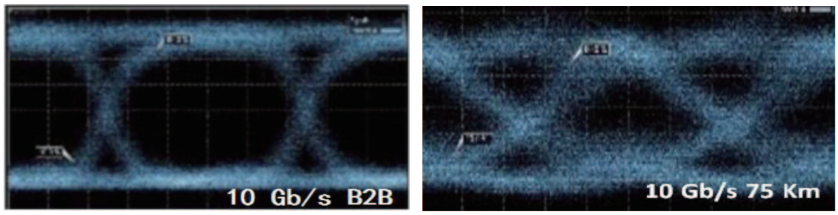

Figure 22 (Color online) Eye diagrams at 10 Gb/s modulation.

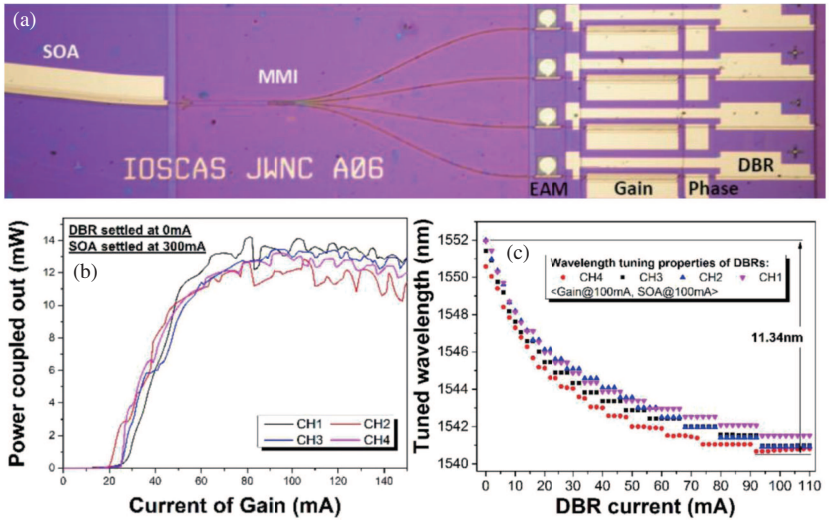

Figure 23 (Color online) (a) Optical graph of a DBR laser array; (b) light output power and (c) tuning properties of the array [48] @Copyright 2016 IEEE.

load balancing that can be flexed according to user demand is highly desirable. High speed is not needed for all users and, for a single user, the required bandwidth usually varies at different time. As a result, there will be different traffic loads for different PON branches, whose bandwidth resources should be varied to meet the users' various needs [47]. Based on the study of discrete DBR lasers, we fabricate EAM modulated widely tunable laser arrays as light sources in optical line terminals (OLTs) of load balanced TWDM-PONs [48]. Figure 23(a) shows a microscope graph of a fabricated four channel DBR laser array. Each DBR laser in the chip consists of a 250-μm long rear DBR section, a 100-μm phase section, a 300-μm gain section, a 50-μm front DBR, and a 150-μm EAM section. To be used as transmitters in OLTs of load balanced WDM-PONs, a wavelength insensitive 4×1 MMI optical combiner is integrated. To compensate for the optical power loss of the passive waveguides, a 600-μm long power booster SOA is adopted. The EAMs are integrated by MQW SAG technique. 1.4-Q materials are butt-jointed as the

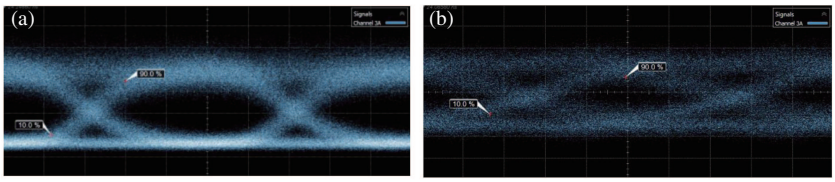

Figure 24 (Color online) 10-Gb/s eye diagrams in (a) BTB configuration and (b) after 50 km fiber transmission.

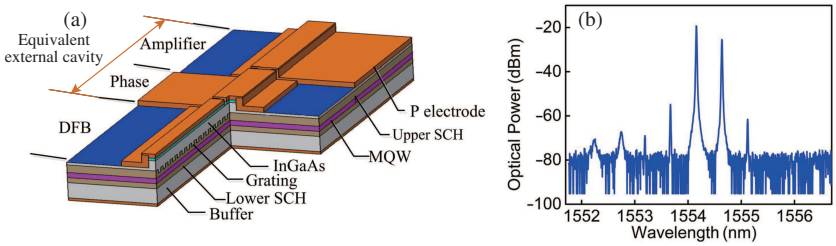

Figure 25 (Color online) (a) Schematic diagram of an AFL; (b) typical dual mode optical spectrum [51] @Copyright 2015 IEEE.

DBR, phase and passive waveguide sections. A shallow and deep ridge waveguide structures are used for the laser and passive waveguide sections, respectively. The size of the chip is 700 μm×2900 μm. The output power and wavelength tuning properties are shown in Figure 23(b) and (c), respectively. The single channel output power can reach above 10 mW with the help of the SOA. The wavelength tuning range of the DBR lasers in the arrays are around 10 nm, which can be enlarged to over 14 nm when the heatsink temperature is varied by 30°C. The small signal modulation bandwidth of the EAMs in the laser array is over 10 GHz. 10-Gb/s transmission over 50 km is performed in standard single mode fiber. The bias voltage of the modulator VEAM = −3.5 V and VPP = 2 V. The measured eye diagrams are shown in Figure 24.

6 Monolithically integrated amplified feedback laser

The amplified feedback laser (AFL) is a simple form of monolithically integrated multi-section semiconductor lasers (MISL) [49]. It consists of a DFB laser section, a phase section, and an amplifier section, as shown in Figure 25(a). The DFB section is the master lasing section. The phase and amplifier sections form an equivalent integrated external cavity. Laser travelling back and forth in the external cavity undergoes a phase and strength adjustment determined by the injection currents at the phase and amplifier sections, respectively. The AFL has a variety of working states depending on the combination of amplifier current $I_{\rm A}$, phase current $I_{\rm P}$ and DFB laser current $I_{\rm DFB}$ [49], whose origin is similar to that of a DFB laser facing an external cavity [50]. One advantage of the integrated feedback cavity in an AFL is that the short equivalent external cavity favors a dual-mode work state (as in Figure 25(b)) having a larger mode separation. By beating two laser modes or sidebands from an AFL on a photodiode, a high-frequency microwave signal whose frequency equals to the mode frequency separation can be generated. By changing the injection currents at the amplifier and phase sections, the wavelengths of the two modes change at different speeds, resulting in a frequency tunable microwave after optoelectronic conversion.

By designing the length of the equivalent external cavity, AFLs with mode separations ranging from 6 to 109 GHz have been demonstrated [49, 51–53], with the capability covering the C, X, K, U, V and W microwave bands. Figure 26(a) shows the frequency down-converted (by 24 GHz) photonic microwave spectra for a 60-GHz AFL in the range from 50 to 72 GHz [51]. The typical -3dB linewidth of the beating microwave is in the range of 2–5 MHz, as shown in Figure 26(b). By using injection locking technique, the photonic microwaves generated directly from the AFL have been used to extract the optical clock from 20 Gb/s [54], 40 Gb/s [55, 56] and 100 Gb/s [57] data stream. A delayed self-injection scheme has been proposed to narrow the beating microwave down to kHz level [58]. To further improve the signal

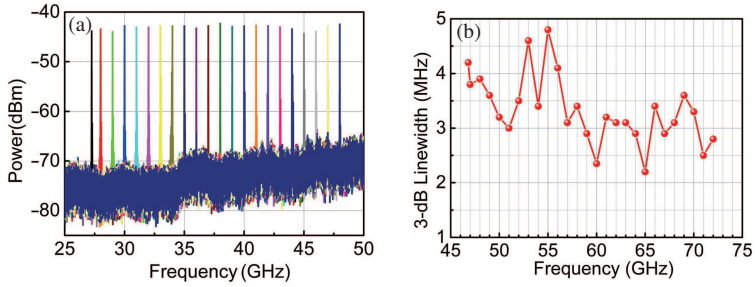

Figure 26 (Color online) (a) Frequency down-converted (by 24 GHz) photonic microwave spectrum corresponding to 50–72 GHz signal; (b) RF power variation and −3-dB linewidth of the photonic microwave generated from a 100G-AFL [51] @Copyright 2015 IEEE.

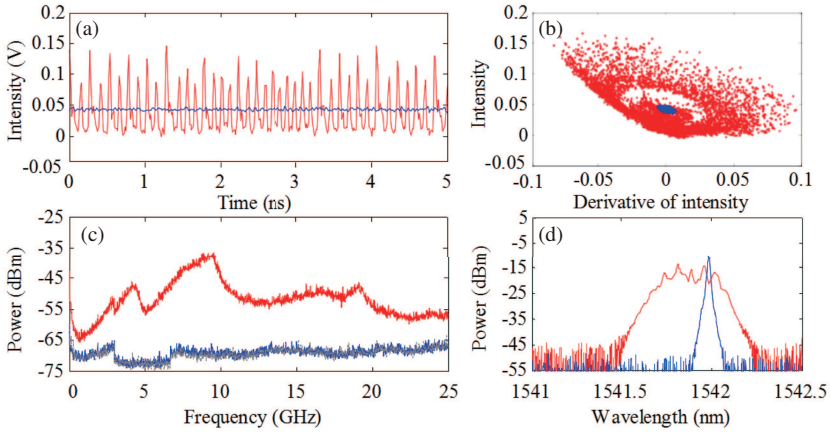

Figure 27 (Color online) (a) The temporal waveform of output; (b) the phase portraits; (c) the RF spectra. The gray line is the noise floor of RF spectrum; (d) the optical spectra of the chaotic AFL. The red color labels the chaotic AFL while the blue color labels single mode AFL [62] @Copyright 2013 OSA.

quality, by using an optoelectronic oscillation configuration, the AFLs are used as the laser source, active photonic filter and modulator, superior microwave signals with phase noise below −106 dBc/Hz @10 kHz offset from 40-GHz carrier are demonstrated [59, 60].

The AFL is also used to generate linearly chirped microwave. By applying a sweeping signal to the amplifier section of the AFL, a linearly chirped microwave waveform with a pulse duration of 1 μs, a bandwidth of 3.3 GHz (ranging from 31.5 to 34.8 GHz), corresponding to a time-bandwidth product of 3.3×10^3 and a compression ratio of 2.6×10^3 are realized [61].

An AFL can also work in a chaos state in which the AFL behaves like a random noise source, generating irregular pulse train in the time domain, having considerably broadened optical and beating RF spectrum, and almost losing its time/spectral coherence. Figure 27 shows the temporal waveform (a), the phase portraits (b), the RF spectrum (c) and the optical spectrum (d) of an AFL working in the chaos state [62]. Even though the time evolution of the chaos is unpredictable, it is a deterministic process determined by the structure and working condition of the AFL. The bandwidth and flatness are two important parameters to evaluate the quality of the of the generated chaos signal. The chaos signal generated from a single AFL can cover a frequency range over 40 GHz, with a standard bandwidth over 16 GHz and flatness of 13 dB. To further improve the bandwidth and flatness, an external optical feedback loop has been introduced, and the route into chaos is chosen to start from the dual-mode state. With this scheme, chaos signal with frequency range extended to over 50 GH, standard bandwidth over 32 GHz, and flatness better than 6.3 dB is demonstrated [63]. Figure 28 shows the generated chaos signal spectrum, the bandwidth and the flatness from an optical-feedback dual-mode AFL. The AFL based chaos generators have been used in high-resolution correlation optical time domain reflectometry (OTDR) [64] and ultra-fast physical random number generation [65]. In the chaotic OTDR experiment, multi-reflection events located in a detection range of 47 km has been precisely located with a range independent resolution

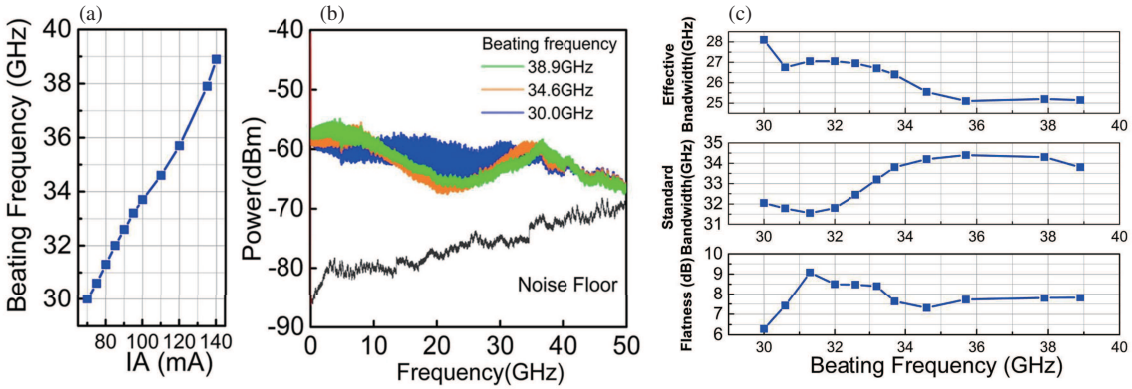

Figure 28 (Color online) (a) Measured free-running beating-frequency; (b) overlapped chaotic spectrums generated by the beating frequencies of 30 GHz (blue line), 34.6 GHz (orange line) and 38.9 GHz (green line); (c) calculated standard bandwidth, effective bandwidths and the flatness as a function of beating frequencies [63] @Copyright 2015 IEEE.

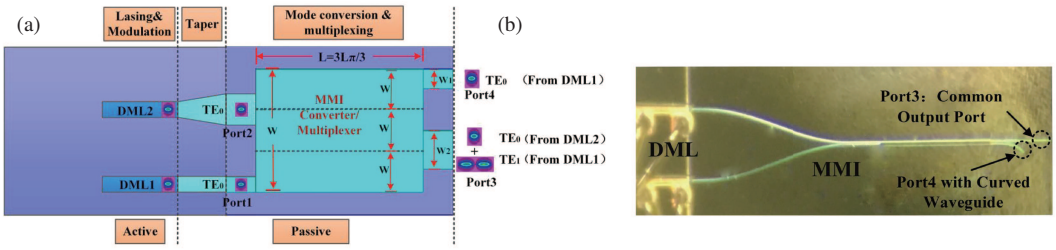

Figure 29 (Color online) (a) Schematic diagram and (b) photograph of the few-mode transmitter. It consists of two directly modulated lasers and a mode converter/multiplexer. DML, directly modulated laser. MMI, multimode interference. $W_{\rm eq}$ is the equivalent MMI width. L_π is the beat length of the two lowest-order modes. W_1 and W_2 are the width of the Port4 and Port3, respectively [66] @Copyright 2018 OSA.

of 2.6 mm. By using 4-least significant bits (LSBs) retaining from the 8-bit digitization of the chaotic waveform, random sequences with a bit rate up to 640 Gbps (160 GS/s×4 bits) are demonstrated.

7 InP-based few-mode transmitter

Space division multiplexing (SDM) or mode division multiplexing (MDM) technology is now gaining popularity among both the academia and the industry. Fiber mode or waveguide mode is used as another degree of freedom in addition to the traditional multiplexing technologies to increase the transmission capacity of communication networks or on-chip systems. The InP platform offers a readily possibility to integrate the laser sources and amplifiers with the mode-manipulation components, making the InP platform very suitable for fully integrated few mode transmitters. An InP-based few-mode transmitter comprising of two directly modulated lasers and a passive MMI based mode converter/multiplexer is demonstrated [66]. The schematic diagram and the photograph of the few-mode transmitter are shown in Figure 29. The two DMLs are DFB lasers, responsible for generating two directly modulated TE_0 modes. The MMI based mode converter/multiplexer converts the TE_0 mode from DML1 to TE_1 mode and multiplexes the TE_1 mode with the TE_0 mode from DML2 at Port3 of the MMI.

The monolithically integrated few mode transmitter works at a wavelength around 1538 nm, with the optical SMSR above 35 dB and small signal modulation bandwidth above 14 GHz. The first row in Figure 30 shows the fundamental TE_0 mode and first-order TE_1 mode generated from the few-mode transmitter. The second row shows the fundamental fiber LP_{01} and first-order fiber LP_{11} mode when a two-mode fiber is illuminated by the TE_0 and TE_1 modes, respectively. The third row shows the eye diagrams of the few-mode transmitter when the two channels are modulated at 10 Gbps, respectively. Error-free performance of the two-mode channels can be obtained for back-to-back BER test. The directly modulated monolithically integrated few-mode transmitter may find potential applications in short range

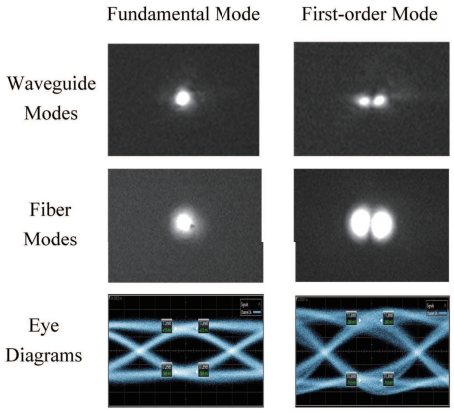

Figure 30 (Color online) The waveguide modes, fiber modes and 10 Gbps eye diagrams of the fundamental and first-order mode generated from the few-mode transmitter [66] @Copyright 2018 OSA.

or on-chip MDM systems where intensity modulation with direct detection (IM/DD) is preferred.

8 Conclusion

In summary, we introduce the fabrication of several kinds of InP-based monolithically integrated laser transmitters. EMLs have been fabricated by a revised SAG process, in which the EAM and laser MQWs can be separately optimized. MWLAs have been fabricated by both SAG of MQWs and SAG of upper SCH layer techniques. Compared with the MWLAs fabricated by the SAG of MQWs technique, the laser arrays by the SCH SAG technique have much better uniformity of wavelength channel spacing, which is comparable to those of the arrays fabricated by EBL technique. What is more, SCH SAG technique is suitable for fabricating laser arrays having less than 0.8-nm channel spacing. Widely tunable directly modulated InP-based DBR lasers are fabricated. By butt-jointing 1.4 Q as DBR material, wavelength tuning range larger than 10 nm can be obtained. DBR lasers with InGaAlAs MQWs as gain material are first fabricated, which have more uniform modulation properties among different wavelength channels than InGaAsP DBR lasers. We also fabricate EAM modulated widely tunable DBR lasers, which have the best wavelength tuning range and output light power for devices with similar structure. Clear-opened eye diagrams can be obtained after 75-km of single mode fiber transmission at 10-Gb/s modulation. Based on discrete DBR lasers, four channel DBR laser arrays have also been fabricated for center station of TWDM-PONs. Monolithically integrated AFLs have been fabricated and have been used for the generation of high quality tunable microwave signal and chaos signals. An InP-based few-mode transmitter comprising of two directly modulated lasers and an MMI based mode converter/multiplexer is demonstrated.

Acknowledgements The work was supported by National Natural Science Foundation of China (NSFC) (Grant Nos. 61635010, 61474112, 61574137, 61320106013, 61335009, 61321063, 61674134, 61274071), National Key Research and Development Program of China (Grant No. 2016YFB0402301), National High Technology Research and Development Program of China (863 Program) (Grant No. 2013AA014502), and National Basic Research Program of China (973 Program) (Grant No. 2014CB340102).

References

1 Kilper D, Bergman K, Chan V W S, et al. Optical networks come of age. Opt Photonic News, 2014, 25: 50–57
2 Nicholes S C, Masanovic M L, Jevremovic B, et al. An 8×8 InP monolithic tunable optical router (MOTOR) packet forwarding chip. J Lightwave Technol, 2010, 28: 641–650
3 Corzine S W, Evans P, Fisher M, et al. Large-scale InP transmitter PICs for PM-DQPSK fiber transmission systems. IEEE Photonic Technol Lett, 2010, 22: 1015–1017
4 Tolstikhin V I, Densmore A, Logvin Y, et al. 44-channel optical power monitor based on an Echelle grating demultiplexer and a waveguide photodetector array monolithically integrated on an InP substrate. In: Proceedings of Optical

Fiber Communications Conference, Atlanta, 2003
5 Tahvili S, Latkowski S, Smalbrugge B, et al. InP-based integrated optical pulse shaper: demonstration of chirp compensation. IEEE Photonic Technol Lett, 2013, 25: 450–453
6 Liang D, Fiorentino M, Srinivasan S, et al. Optimization of hybrid silicon microring lasers. IEEE Photonic J, 2011, 3: 580–587
7 Kurczveil G, Heck M J, Peters J D, et al. An integrated hybrid silicon multiwavelength AWG laser. IEEE J Sel Top Quant Electron, 2011, 17: 1521–1527
8 Srinivasan S, Tang Y, Read G, et al. Hybrid silicon devices for energy-efficient optical transmitters. IEEE Micro, 2013, 33: 22–31
9 Arafin S, Coldren L A. Advanced InP photonic integrated circuits for communication and sensing. IEEE J Sel Top Quant Electron, 2018, 24: 6100612
10 Kihara T, Nitta Y, Suda H, et al. Wavelength control of arrayed waveguide by MOVPE selective area growth. J Cryst Growth, 2000, 221: 196–200
11 Sasaki T, Yamaguchi M, Kitamura M. Monolithically integrated multi-wavelength MQW-DBR laser diodes fabricated by selective metalorganic vapor phase epitaxy. J Cryst Growth, 1994, 145: 846–851
12 Kobayashi W, Arai M, Yamanaka T, et al. Design and fabrication of 10-/40-Gb/s, uncooled electroabsorption modulator integrated DFB laser with butt-joint structure. J Lightwave Technol, 2010, 28: 164–171
13 Cheng Y B, Pan J Q, Liang S, et al. Butt-coupled MOVPE growth for high-performance electro-absorption modulator integrated with a DFB laser. J Cryst Growth, 2007, 308: 297–301
14 Cheng Y B, Pan J Q, Wang Y, et al. 40-Gb/s low chirp electroabsorption modulator integrated with DFB laser. IEEE Photonic Technol Lett, 2009, 21: 356–358
15 Zhu H L, Liang S, Zhao L J, et al. A selective area growth double stack active layer electroabsorption modulator integrated with a distributed feedback laser. Chinese Sci Bull, 2009, 54: 3627–3632
16 Deng Q F, Zhu H L, Xie X, et al. Low chirp EMLs fabricated by combining SAG and double stack active layer techniques. IEEE Photonic J, 2018, 10: 7902007
17 Zah C E, Amersfoort M R, Pathak B N, et al. Multiwavelength DFB laser arrays with integrated combiner and optical amplifier for WDM optical networks. IEEE J Sel Top Quant Electron, 1997, 3: 584–597
18 Corzine S W, Evans P, Fisher M, et al. Large-scale InP transmitter PICs for PM-DQPSK fiber transmission systems. IEEE Photonic Technol Lett, 2010, 22: 1015–1017
19 Li G P, Makino T, Sarangan A, et al. 16-wavelength gain-coupled DFB laser array with fine tunability. IEEE Photonic Technol Lett, 1996, 8: 22–24
20 Young M G, Koren U, Miller B I, et al. A 16×1 wavelength division multiplexer with integrated distributed Bragg reflector lasers and electroabsorption modulators. IEEE Photonic Technol Lett, 1993, 5: 908–910
21 Zhang C, Liang S, Zhu H L, et al. The fabrication of 10-channel DFB laser array by SAG technology. Opt Commun, 2013, 311: 6–10
22 Zhang C, Liang S, Zhu H L, et al. Multi-channel DFB laser arrays fabricated by SAG technology. Opt Commun, 2013, 300: 230–235
23 Zhang C, Liang S, Ma L, et al. Multi-channel DFB laser array fabricated by SAG with optimized epitaxy conditions. Chin Opt Lett, 2013, 11: 041401
24 Zhang C, Zhu H L, Liang S, et al. Monolithically integrated 4-channel-selectable light sources fabricated by the SAG technology. IEEE Photonic J, 2013, 5: 1400407
25 Zhang C, Zhu H L, Liang S, et al. Ten-channel InP-based large-scale photonic integrated transmitter fabricated by SAG technology. Opt Laser Technol, 2014, 64: 17–22
26 Xu J, Liang S, Zhang Z, et al. EML array fabricated by SAG technique monolithically integrated with a buried ridge AWG multiplexer. Opt Laser Technol, 2017, 91: 46–50
27 Zhang C, Liang S, Zhu H L, et al. A modified SAG technique for the fabrication of DWDM DFB laser arrays with highly uniform wavelength spacings. Opt Express, 2012, 20: 29620–29625
28 Zhang C, Liang S, Zhu H L, et al. Multichannel DFB laser arrays fabricated by upper SCH layer SAG technique. IEEE J Quant Electron, 2014, 50: 92–97
29 Xu J J, Liang S, Qiao L J, et al. Laser arrays with 25-GHz channel spacing fabricated by combining SAG and REC techniques. IEEE Photonic Technol Lett, 2016, 28: 2249–2252
30 Shi Y C, Li S M, Li L Y, et al. Study of the multiwavelength DFB semiconductor laser array based on the reconstruction-equivalent-chirp technique. J Lightwave Technol, 2013, 31: 3243–3250
31 Tohmori Y, Jiang X, Arai S, et al. Novel structure GaInAsP/InP 1.5–1.6 μm bundle integrated-guide (BIG) distributed bragg reflector laser. Jpn J Appl Phys, 1985, 24: 399–401
32 Han L S, Liang S, Wang H T, et al. Fabrication of low-cost multiwavelength laser arrays for OLTs in WDM-PONs by combining the SAG and BIG techniques. IEEE Photonic J, 2015, 7: 1–7
33 Park S J, Lee C H, Jeong K T, et al. Fiber-to-the-home services based on wavelength-division-multiplexing passive optical network. J Lightwave Technol, 2004, 22: 2582–2591
34 Banerjee A, Park Y, Clarke F, et al. Wavelength-division-multiplexed passive optical network (WDM-PON) technologies for broadband access: a review. J Opt Netw, 2005, 4: 737–758
35 Ponzini F, Cavaliere F, Berrettini G, et al. Evolution scenario toward WDM-PON. J Opt Commun Netw, 2009, 1: 25–34
36 Raring J W, Johansson L A, Skogen E J, et al. 40-Gb/s widely tunable low-drive-voltage electroabsorption-modulated

transmitters. J Lightwave Technol, 2007, 25: 239–248
37 Johnson J E, Ketelsen L J P, Geary J M, et al. 10 Gb/s transmission using an electroabsorption-modulated distributed Bragg reflector laser with integrated semiconductor optical amplifier. In: Proceedings of Optical Fiber Communication Conference and Exhibit, Anaheim, 2013
38 Kim S B, Sim J S, Kim K S, et al. Selective-area MOVPE growth for 10 Gbit/s electroabsorption modulator integrated with a tunable DBR laser. J Cryst Growth, 2007, 298: 672–675
39 Weber J P. Optimization of the carrier-induced effective index change in InGaAsP waveguides-application to tunable Bragg filters. IEEE J Quant Electron, 1994, 30: 1801–1816
40 Han L S, Liang S, Zhang C, et al. Fabrication of widely tunable ridge waveguide DBR lasers for WDM-PON. Chinese Opt Lett, 2014, 12: 091402
41 Yu L Q, Wang H T, Lu D, et al. A widely tunable directly modulated DBR laser with high linearity. IEEE Photonic J, 2014, 6: 1501308
42 Zhang C, Liang S, Zhu H L, et al. Widely tunable dual-mode distributed feedback laser fabricated by selective area growth technology integrated with Ti heaters. Opt Lett, 2013, 38: 3050–3053
43 Zhang C, Liang S, Zhu H L, et al. Tunable DFB lasers integrated with Ti thin film heaters fabricated with a simple procedure. Opt Laser Technol, 2013, 54: 148–150
44 Han L H, Liang S, Xu J J, et al. DBR laser with over 20 nm wavelength tuning range. IEEE Photonic Technol Lett, 2016, 28: 943–946
45 Zhou D B, Liang S, Zhao L J, et al. High-speed directly modulated widely tunable two-section InGaAlAs DBR lasers. Opt Express, 2017, 25: 2341–2346
46 Han L H, Liang S, Wang H T, et al. Electroabsorption-modulated widely tunable DBR laser transmitter for WDM-PONs. Opt Express, 2014, 22: 30368–30376
47 Hara K, Nakamura H, Kimura S, et al. Flexible load balancing technique using dynamic wavelength bandwidth allocation (DWBA) toward 100 Gbit/s-class-WDM/TDM-PON. In: Proceedings of the 36th European Conference and Exhibition on Optical Communication, Torino, 2010
48 Xu J J, Han L S, Hou L P, et al. EAM modulated DBR laser array for TWDM-PON applications. In: Proceedings of IEEE Photonics Conference (IPC), Waikoloa, 2016
49 Yu L Q, Lu D, Pan B W, et al. Monolithically integrated amplified feedback lasers for high-quality microwave and broadband chaos generation. J Lightwave Technol, 2014, 32: 3595–3601
50 Lang R, Kobayashi K. External optical feedback effects on semiconductor injection laser properties. IEEE J Quant Electron, 1980, 16: 347–355
51 Pan B W, Lu D, Zhang L M, et al. Widely tunable amplified feedback laser with beating-frequency covering 60-GHz band. IEEE Photonic Technol Lett, 2015, 27: 2103–2106
52 Pan B W, Yu L Q, Lu D, et al. Simulation and experimental characterization of a dual-mode two-section amplified feedback laser with mode separation over 100 GHz. Chinese Opt Lett, 2014, 12: 110605–110609
53 Pan B W, Guo L, Zhang L M, et al. Widely tunable monolithic dual-mode laser for W-band photonic millimeter-wave generation and all-optical clock recovery. Appl Opt, 2016, 55: 2930–2935
54 Sun Y, Pan J Q, Zhao L J, et al. All-optical clock recovery for 20 Gb/s using an amplified feedback DFB laser. J Lightwave Technol, 2010, 28: 2521–2525
55 Wang L, Zhao X F, Lou C Y, et al. 40 Gbits/s all-optical clock recovery for degraded signals using an amplified feedback laser. Appl Opt, 2010, 49: 6577–6581
56 Qiu J F, Chen C, Zhao L J, et al. Detailed analysis of a 40 GHz all-optical synchronization based on an amplified-feedback distributed feedback laser. Appl Opt, 2012, 51: 2894–2901
57 Pan B W, Yu L Q, Guo L, et al. 100 Gb/s all-optical clock recovery based on a monolithic dual-mode DBR laser. Chin Opt Lett, 2016, 14: 030604–030607
58 Pan B W, Lu D, Sun Y, et al. Tunable optical microwave generation using self-injection locked monolithic dual-wavelength amplified feedback laser. Opt Lett, 2014, 39: 6395–6398
59 Lu D, Pan B W, Chen H B, et al. Frequency-tunable optoelectronic oscillator using a dual-mode amplified feedback laser as an electrically controlled active microwave photonic filter. Opt Lett, 2015, 40: 4340–4343
60 Pan B W, Lu D, Zhang L M, et al. A widely tunable optoelectronic oscillator based on directly modulated dual-mode laser. IEEE Photonic J, 2015, 7: 1–7
61 Guo L, Zhang R K, Lu D, et al. Linearly chirped microwave generation using a monolithic integrated amplified feedback laser. IEEE Photonic Technol Lett, 2017, 29: 1915–1918
62 Wu J G, Zhao L J, Wu Z M, et al. Direct generation of broadband chaos by a monolithic integrated semiconductor laser chip. Opt Express, 2013, 21: 23358–23364
63 Pan B W, Lu D, Zhao L J. Broadband chaos generation using monolithic dual-mode laser with optical feedback. IEEE Photonic Technol Lett, 2015, 27: 2516–2519
64 Zhang L M, Pan B W, Chen G C, et al. Long-range and high-resolution correlation optical time-domain reflectometry using a monolithic integrated broadband chaotic laser. Appl Opt, 2017, 56: 1253–1256
65 Zhang L M, Pan B W, Chen G C, et al. 640-Gbit/s fast physical random number generation using a broadband chaotic semiconductor laser. Sci Rep, 2017, 8: 45900
66 Li Z S, Lu D, He Y M, et al. InP-based directly modulated monolithic integrated few-mode transmitter. Photonic Res, 2018, 6: 463–467